DOI: 10.1002/ ((please add manuscript number))
Article type: Full Paper

$AgFeS_2$ Nanowires Modified $BiVO_4$ Photoanode for Photoelectrochemical Water Splitting

Xiuzhen Zheng[a], Beniamino Sciacca[b], Erik C. Garnett[b], Liwu Zhang[a]**

[a]Shanghai Key Laboratory of Atmospheric Particle Pollution and Prevention, Department of Environmental Science and Engineering
Fudan University
Shanghai, 200433, P. R. China
E-mail: zhanglw@fudan.edu.cn.
[b]Center for Nanophotonics
FOM Institute AMOLF
Science Park Amsterdam 104, 1098 XG Amsterdam, The Netherlands
E-mail: e.garnett@amolf.nl

Keywords: ternary sensitizer, extended light absorption, PEC, composite, solar-to-hydrogen

Abstract

Photoelectrochemical water splitting is a very promising and environmentally friendly route for the conversion of solar energy into hydrogen. However, the solar-to-hydrogen conversion efficiency is still very low due to limited light absorption and rapid bulk recombination of charge carriers. In this work, we present a novel ternary sensitizer $AgFeS_2$, with a narrow band gap of 0.9 eV, combined with $BiVO_4$ to enhance the solar-to-hydrogen energy conversion efficiency. The photoelectrochemical properties of $AgFeS_2/BiVO_4$ electrode are investigated and the photocurrent densities of $AgFeS_2/BiVO_4$ composite electrodes are greatly enhanced compared with prestine $BiVO_4$ (15 times higher at 0.6 V vs. Ag/AgCl under AM 1.5 G illumination). The enhanced photoelectrochemical properties stem from the extended light absorption spectrum, fast charge transfer and appropriate energy gap alignment. It is demonstrated that $AgFeS_2$ nanowire is a promising inorganic sensitizer for improving the solar water splitting efficiency.

1. Introduction

Since the discovery of water splitting on titanium dioxide (TiO_2) surface by photoirradiation, photoelectrochemical (PEC) technology has attracted extensive interest. [1] After decades of development, it has made great progress in the H_2 production of water splitting, degradation of organic pollutants and CO_2 reduction. [2-5] However, the PEC efficiency is still low, seriously restricting its wide application in solving the energy shortage and environmental pollution problems. Exploring new and efficient photoelectrodes is proved to be an important strategy for improving PEC efficiency and promoting the practical application of PEC technology. Among photoelectrode materials, bismuth vanadate ($BiVO_4$) is one of the leading metal oxides, with a direct bandgap of 2.3～2.4 eV and a suitable valence band position for O_2 evolution. [6] $BiVO_4$ was first reported by Kudo and coworkers as a photocatalyst for water oxidation. [7] Since then $BiVO_4$ has been widely investigated as a visible-light-driven photocatalyst for water oxidation and organic compound degradation. [8–12] Recently, extensive attention has focused on $BiVO_4$ as a photoanode for PEC water splitting. [13–16] However, the activity of pure $BiVO_4$ is low due to its poor light absorptive performance and difficult migration of electron-hole pairs, which has been demonstrated by van de Krol and coworkers. [17] Therefore, poor electron transport results in high bulk recombination of photogenerated charge carriers and a low solar-to-hydrogen conversion efficiency.

To address these issues, many attempts have been made to modify the bulk electronic properties of $BiVO_4$ photocatalysts, such as noble metals coating, elemental doping and narrow bandgap semiconductors combining. [15, 18-23] Among these methods, one of the most efficient ways is to deposit a sensitizer with appropriate band gap on $BiVO_4$. The sensitizer not only extends the light absorption spectrum, but also accelerates photogenerated electron–hole separation. Ternary I-III-VI_2 semiconductors have been regarded as one of the most promising materials for thin film sensitizer because of their unique properties, large absorption coefficients, high conversion efficiency, and low toxicity. [24] Silver iron sulfide

($AgFeS_2$, Lenaite) is a novel ternary I-III-VI_2 semiconductor, which has a narrow band gap (about 0.9 eV) covering the entire visible spectrum and also has a high absorption coefficient. [25] Han et al. and Sciacca et al. successfully obtained $AgFeS_2$ via different synthetic pathways. [25, 26] To the best of our knowledge, there has been no report on PEC electrode made from $BiVO_4$ modified with ternary $AgFeS_2$ so far. This study extends the work to a new coupled photoanode made of ternary sensitizer $AgFeS_2$ and $BiVO_4$.

We have successfully prepared the $AgFeS_2$/ $BiVO_4$ composite by incorporating $AgFeS_2$ with $BiVO_4$ film via a simple drop-coating method. The composite of $AgFeS_2$ and $BiVO_4$ semiconductors with appropriate oxidation reduction energy levels can enhance the charge separation and engender its wide spectral response by extension of light absorption in the visible region. In this study, ternary $AgFeS_2$ sensitizer modified $BiVO_4$ is fabricated on fluorine-tin-oxide (FTO) substrate and applied as photoanode. The expected enhanced PEC properties of $AgFeS_2/BiVO_4$ composite is confirmed by hydrogen and oxygen evolution from solar water splitting. The mechanism for the enhanced PEC performance and gas evolution on $AgFeS_2/BiVO_4$ composite is discussed in detail.

2. Results and Discussion

2.1. Fabrication and Characterization of $AgFeS_2/BiVO_4$ Composite Electrodes

Scanning electron microscope (SEM) is employed to investigate the morphology of the as-prepared $AgFeS_2$, $BiVO_4$ and $AgFeS_2/BiVO_4$ samples (**Figure 1**). Figure 1a shows the typical morphology of $AgFeS_2$. It is comprised of nanowires, and the length is about ten micrometers. Meanwhile, the morphology of the $BiVO_4$ (Figure S1, Supporting information) is also investigated, which is comprised of nanoparticles with diameter from 100 to 400 nm. Herein, $AgFeS_2$ nanowires are firstly prepared via a solution phase conversion of metallic Ag nanowires from our previous report. [25] The as-prepared $AgFeS_2$ nanowires are then stirred in ethanol for 24 hrs to form suspension, which are dropped onto the $BiVO_4$ film to obtain

$AgFeS_2/BiVO_4$ composites. According to the amount of $AgFeS_2$ (10, 20, 30, 40 and 50 μL) being added on the $BiVO_4$ samples, the corresponding $AgFeS_2/BiVO_4$ samples are labeled as AB-10, AB-20, AB-30, AB-40 and AB-50, respectively. As the morphologies of $AgFeS_2/BiVO_4$ samples with different amount of $AgFeS_2$ are almost the same, only the coverage of $AgFeS_2$ on $BiVO_4$ is different. While the photocurrent density of AB-40 electrode is higher than other $AgFeS_2/BiVO_4$ samples, it is thus chosen as the example for the SEM and energy-dispersive X-ray (EDX) measurements. In the AB-40 sample, it is clearly observed that $AgFeS_2$ nanowires are on the top surface of $BiVO_4$ (Figure 1b and S2). Additionally, EDX mapping obtained in SEM mode (**Figure 2**) is performed to confirm the composition of AB-40. As seen from the SEM image (Figure 2a), $AgFeS_2$ nanowires are nanocrystalline, which is confirmed by electron diffraction in our previous synthetic study. [25] Moreover, the Ag, Fe, and S elements (Figure 2b-d) are distributed homogeneously along the nanowires, indicating the existence of $AgFeS_2$. Bi, V and O (Figure 2e-g) elements are also detected, which come from the $BiVO_4$ substrate. The composite structure of $AgFeS_2/BiVO_4$ is thus confirmed by the SEM and EDX studies.

The crystal structure of $BiVO_4$ and AB-40 are determined by XRD, as shown in **Figure 3**. The XRD pattern of $BiVO_4$ can be matched to monoclinic $BiVO_4$ (JCPDS No. 14–0688), and the FTO film (JCPDS No. 41-1445) is shown in Figure S3. The 2θ diffraction peaks of 28.8°, 30.5°, 34.5°, 35.2°, 39.8° and 42.5° can be respectively indexed as (121), (040), (200), (002), (211), and (051) planes of monoclinic $BiVO_4$ structure, which is consistent with the literature. [27] Moreover, the 2θ diffraction peaks and corresponding planes of $AgFeS_2$ (JCPDS No. 48-1895) are shown in Figure S4. It is noteworthy that $AgFeS_2$ is clearly observed in the XRD pattern of the AB-40 sample. Based on the results of SEM images, elemental mapping and XRD patterns, it is clear that the $AgFeS_2/BiVO_4$ composite is successful prepared via a simple drop-coating approach.

It is well known that light absorption of the photoelectrode materials plays an important role in the solar water splitting. The UV−vis diffuse reflection spectra of $BiVO_4$, $AgFeS_2$, and $AgFeS_2/BiVO_4$ composites with different $AgFeS_2$ contents are thus studied. The optical band gap energy (E_g) of $BiVO_4$ (Figure S5) is obtained by using the equation of $(F(R)\ E)^{1/2} = A\ (E-E_g)$. [28] The estimated band gap value of $BiVO_4$ as a direct band semiconductor is 2.32 eV, which is in agreement with the previous reports. [7, 8] To further analyze the diffuse reflection spectra of $AgFeS_2/BiVO_4$ composites (**Figure 4**), it can be found that there are obvious enhancements in the light absorption of $AgFeS_2/BiVO_4$ composites, compared with the bare $BiVO_4$. This is due to the fact that $AgFeS_2$ with its narrow band gap (0.88 eV) significantly extends the light absorption range of $AgFeS_2/BiVO_4$ composites. With the introduction of $AgFeS_2$, a more efficient utilization of the solar spectrum on $AgFeS_2/BiVO_4$ can be achieved, which is helpful to improve the PEC properties and facilitates its use in practical solar water splitting. The $AgFeS_2$/FTO film is prepared by adding $AgFeS_2$ suspension onto FTO until it is fully covered with $AgFeS_2$ sample. Therefore, the amount of $AgFeS_2$ on the FTO substrate is higher than the other samples, this is the reason that $AgFeS_2$ film has much lower %R.

2.2. Photoelectrochemical Properties of $AgFeS_2/BiVO_4$ Electrodes

Photocurrent densities as a function of applied potential of $AgFeS_2$, $BiVO_4$ and $AgFeS_2/BiVO_4$ electrodes are investigated by linear sweep photovoltammetry (LSV), which demonstrates the electron generation capacity and electron transfer effectiveness. The photocurrent responses of $AgFeS_2$, $BiVO_4$ and $AgFeS_2/BiVO_4$ photoelectrodes (**Figure 5**) are studied under AM 1.5G illumination (100 mW/cm^2). Figure 5a shows the LSV (scan rate: 10 mV/s) on the $BiVO_4$, $AgFeS_2$ and $AgFeS_2/BiVO_4$ photoanodes under light illumination from the backside (FTO side) of the electrodes. The anodic photocurrents increase steadily with the applied positive potential, and an enhanced photocurrent for the $AgFeS_2/BiVO_4$ composite electrodes is obtained essentially over the entire potential range compared with $BiVO_4$ electrode. The AB-40 electrode shows the maximum enhancement among all of the electrodes,

and the current in the dark is negligible. This significant improvement in photocurrent could be attributed to the effect of $AgFeS_2$ modification. It is also notable that prestine $AgFeS_2$ shows a very low photocurrent. The LSVs of the photoanodes under chopped illumination are also studied and shown a similar trend in Figure 5b. Herein, the $BiVO_4$ photoanode demonstrates low photocurrent, which is largely lower than most of the previous reports in the literature on $BiVO_4$ photoelectrodes.[29, 30] The poor PEC performance is mainly caused by non-uniform distribution of the $BiVO_4$ nanoparticles on the FTO surface, which is not fully covered by $BiVO_4$ nanoparticles. It is thus anticipated that the photocurrent of $AgFeS_2/BiVO_4$ composite would be much higher if $BiVO_4$ substrate with better quality is employed.

Additional photoelectrochemical measurements (**Figure 6**) are performed to further investigate the enhancement mechanism for water splitting of $AgFeS_2/BiVO_4$ composite electrode. Figure 6a shows the photocurrent versus time curves (0.6 V vs. Ag/AgCl under AM 1.5 G illumination) for the samples with several on-off cycles. The photocurrent responses of the $AgFeS_2/BiVO_4$ composite films are higher than that of $BiVO_4$ and $AgFeS_2$, and AB-40 possesses the highest photocurrent among them, which is almost 15 times higher than that of $BiVO_4$. As shown in Figure 6b, it is clearly shown that the radius of the arc on the electrochemical impedance spectroscopy (EIS) Nynquist plots of $AgFeS_2/BiVO_4$ samples are smaller than that of the $BiVO_4$, which reflect that $AgFeS_2/BiVO_4$ possessed faster interfacial charge transfer. The results are in good agreement with the photocurrent measurements. According to the photocurrent graphs and EIS plots, it indicates that the presence of $AgFeS_2$ in the $AgFeS_2/BiVO_4$ composite is capable of improving separation efficiency and effectively inhibiting the recombination of photogenerated electron-hole pairs. Such an explanation would also make more sense given its small bandgap, which means it shouldn’t participate directly in water splitting.

To further gain a qualitative understanding of the charge recombination behavior in $BiVO_4$ and AB-40, the transient photocurrent decay occurring immediately upon illumination is

investigated (Figure 6c). Transient photocurrent response has been demonstrated to be a useful technique for investigating the efficiency of the separation of photogenerated electron–hole pairs. [31] The photocurrent curve initially presents a spike and then the spike gradually decays until the photocurrent reaches a stable value. The decrease in the photocurrent indicates that recombination is occurring within the $AgFeS_2/BiVO_4$ electrode. When the light is switched on, a photocurrent spike is observed at an applied potential of 0.6 V vs. Ag/AgCl due to the sudden generation of charge carriers, which then recombine after generation. Charge recombination can be caused either by accumulation of electrons in the bulk or accumulation of holes at the surface. The accumulation of holes would cause an equally large cathodic transient when the light is switched off and electrons in the conduction band react with the accumulated holes. [9] However, cathodic transients can barely be observed, indicating accumulation of holes are not the main recombination process in $BiVO_4$ film and AB-40 electrodes. The transients in Figure 6c are thus attributed to the accumulation of electrons due to the poor electron transportation in $BiVO_4$, which is consistent with the results observed in the previous reports. [14] The transient decay time can be calculated from a logarithmic plot of parameter *D*, given by the equation [32, 33]:

$$D = (I_t - I_s) / (I_m - I_s) \quad (1)$$

where I_m is the photocurrent spike, I_t is the photocurrent at time t and I_s is the steady state photocurrent. I_s is achieved as the recombination and charge generation reaches equilibrium. The transient decay time is defined as the time at which $\ln D = -1$. [32] Therefore, based on the photocurrent profiles measured in Figure 6c, the transient decay times of $BiVO_4$ film and AB-40 electrodes are calculated and plotted in Figure 6d. The transient decay time for AB-40 electrode is 1.87 s, which is more than three times longer than the transient decay time of $BiVO_4$ film (0.49 s). Generally, the photocurrent decay rate is determined by charge carrier recombination rate. [33] Therefore, we expect that a slower recombination rate gives rise to a longer transient decay time and a significantly longer transient decay time is observed for the

AB-40, suggesting a lower charge carrier recombination rate in the AB-40 compared to the $BiVO_4$ film.

In order to address the quantitative correlation between $AgFeS_2$ sensitization and light absorption of $AgFeS_2/BiVO_4$ composite, incident-photon-to-current-conversion efficiency (IPCE) measurements are performed to study the photoactive wavelength regime for $AgFeS_2$, $BiVO_4$ and AB-40 (**Figure 7**). IPCE can be expressed as: [34, 35]

$$IPCE = (1240 \times I) / (\lambda \times J_{light}) \quad (2)$$

where I is the photocurrent density, λ is the incident light wavelength, and J_{light} is the measured irradiance. For $AgFeS_2$ itself, the IPCE data is very low, which is consistent with the photocurrent data. The IPCE plots of $BiVO_4$ and AB-40 look similar and strongly decrease upon excitation at longer wavelengths, the $BiVO_4$ shows a minimal photoresponse below the bandgap energy (~2.32 eV, 535 nm), while the composite electrode (AB-40) shows a significant red shift toward lower energy. For example, at above-bandgap illumination, the IPCE of pure $BiVO_4$ and AB-40 samples at the incident wavelength of 500 nm are 1.03% and 6.59%, indicating the presence of $AgFeS_2$ can improve the charge separation efficiency and thus an enhanced photoresponse. At below bandgap illumination of 550 nm, the IPCE of AB-40 is around 5%, while prestine $BiVO_4$ shows no photoresponse. This is the direct evidence that $AgFeS_2$ can also act as a photosensitizer and substantially improves the light collection and conversion efficiency in the visible region.

To verify that the measured photocurrent of the photoanodes originated from water splitting rather than any other undesired side reactions, a water splitting experiment is performed at 1.6 V on the AB-40 photoanode, and the gas evolution (**Figure 8**) and corresponding photocurrent response (Figure S6) are measured. The ratio of evolution rates of H_2 and O_2 is close to the stoichiometric value of 2.0, with rates of 9.1 ± 0.1 μmol h^{-1} cm^{-2} for H_2 and 4.3 ± 0.1 μmol h^{-1} cm^{-2} for O_2. Assuming 100% Faradaic efficiency, at a photocurrent of 0.60 mA cm^{-2}, the evolution rates of H_2 and O_2 should be 10.6 μmol h^{-1} cm^{-2} and 5.3 μmol h^{-1} cm^{-2},

respectively. Hence the faradaic efficiencies for H_2 and O_2 are more than 80%, indicating that the observed photocurrent could be mostly attributed to water splitting. Additionally, the photocurrent of AB-40 only very slightly decreases after 3 hrs of water splitting experiment (Figure S6), implying the high stability of the $AgFeS_2/BiVO_4$ composite photoanode. It can be concluded that $AgFeS_2$ is relatively stable and promising as a sensitizer for solar water splitting.

2.3. Photoelectrochemical Mechanism for the Water Splitting over $AgFeS_2/BiVO_4$ Composite Photoanode

Based on the above data, a possible mechanism for the water splitting over $AgFeS_2/BiVO_4$ composite photoanode under light irradiation can be proposed. Here $AgFeS_2$ serves as a sensitizer for light-induced redox process while $BiVO_4$ is a substrate. The band gap of $BiVO_4$ is evaluated as 2.32 eV from the UV-vis spectrum, which is consistent with literature reports. The corresponding conduction band (E_{CB}) and valence band positions (E_{VB}) of $BiVO_4$ and $AgFeS_2$ at the point of zero charge are presumed through the following equations [36, 37]:

$$\chi = 1/2(A_f + I_1) \quad (3)$$

$$E_{CB} = \chi - E_0 - 1/2E_g \quad (4)$$

where χ is the bulk electronegativity of the compound, defined as the arithmetic mean of the atomic electron affinity and the first ionization energy (for BiVO4, χ is 6.04 eV [37, 38]; for $AgFeS_2$, χ is 5.14 eV [36]). E_0 is the energy of free electrons on the hydrogen scale (about 4.5 eV), and E_g is the band gap energy of the semiconductor. The position of the valence band edge is determined by $E_{VB} = E_{CB} + E_g$. The calculated result shows that the bottom of the conduction band of $BiVO_4$ is around 0.4 eV versus normal hydrogen electrode (NHE), while the top of the valence band is around 2.7 eV. Meanwhile, the value of E_{CB} measured (Figure S7) by photocurrent onset potential is accorded with the calculated result. The calculated conduction band and valence band positions (vs. NHE) of $AgFeS_2$ and $BiVO_4$ are listed in **Table 1**.

The energy band diagram of the $AgFeS_2/BiVO_4$ composite photoanode is presented in **Figure 9**. The difference in E_{CB} between $AgFeS_2$ and $BiVO_4$ allows for the transfer of electrons from the conduction band of $AgFeS_2$ to that of $BiVO_4$. Upon light irradiation ($\lambda <$ 535 nm), both the $AgFeS_2$ and $BiVO_4$ components generate electron-hole pairs, although the majority from the $BiVO_4$ due to its large excess. Whereas the electrons are able to move easily to the FTO contact, the holes are expected to be left on the surface of $AgFeS_2/BiVO_4$ photoanode. This improved charge separation efficiency leads to the improved water oxidation. On the other hand, under light irradiation beyond the absorption edge of $BiVO_4$ ($\lambda >$ 535 nm), the electrons photogenerated in $AgFeS_2$ due to its small band gap can readily transfer to the conduction band of $BiVO_4$, which improves the charge carrier separation in $AgFeS_2$. $AgFeS_2$ itself is unable to directly split water toward O_2 due to the unfavorable position of valence band with respect to the O_2/H_2O redox potential. However, the holes trapped at the $AgFeS_2$ component can react with H_2O to form OH radicals ($H_2O + h^+ \rightarrow OH\bullet + H^+$).[39] OH radicals are highly reactive and, in absence of other species, can couple with another OH radical to form H_2O_2 ($2OH\bullet \rightarrow H_2O_2$). [40] Hydrogen peroxide is known to decompose spontaneously to O_2 and water, and H_2O_2 can also be photo-oxidized by holes in $BiVO_4$ ($H_2O_2 + h^+ \rightarrow O_2 + H^+ + 4e^-$). [41-43] In conclusion, photogenerated holes formed in both $BiVO_4$ and $AgFeS_2$, following different pathways, can react with water to form O_2 which results in higher number of collected photoelectrons, [44, 45] then used for the H_2 production in the cathodic electrode.

4. Conclusions

$AgFeS_2$ nanowire/$BiVO_4$ composite photoelectrodes are fabricated via a facile drop-coating method. $AgFeS_2$ nanowire, with a narrow band gap of 0.9 eV, as a novel ternary sensitizer to improve the water splitting efficiency of $BiVO_4$ photoanode is demonstrated. The photocurrent density of $AgFeS_2/BiVO_4$ electrode is greatly enhanced compared with prestine

$BiVO_4$ electrode (15 times higher at 0.6 V vs. Ag/AgCl under AM 1.5 G illumination). The excellent photoelectrochemical properties stem from the extended light absorption spectrum and improved charge separation and collection efficiency. Furthermore, hydrogen and oxygen production on $AgFeS_2/BiVO_4$ electrodes is measured and these composite photoelectrodes are found to be promising for solar water splitting. $AgFeS_2$ drastically improves the solar water splitting efficiency of $BiVO_4$ photoanodes, suggesting $AgFeS_2$ as a new effective sensitizer for improving the efficiency of solar-to-fuel energy conversion. Further work on preparing more active $BiVO_4$ substrate and more stable $AgFeS_2$ by surface modification is being carried out in our lab.

4. Experimental section

Preparation of the $AgFeS_2/BiVO_4$ composite: The $AgFeS_2$ nanowires were obtained using a modified synthesis from our previous report, optimized further for larger scale reactions with higher yield.[25] In a typical reaction, 90 mL of DMSO was placed in a round bottom flask. 102 mg of $FeCl_2 \cdot 4H_2O$, 100 μL of thioglycolic acid and 2.5 mL of 20 g/L Ag nanowire solution were added to the DMSO. N_2 was bubbled for 30 min to remove oxygen. Subsequently, 10 mL of water with 451 mg of $Na_2S_2O_3 \cdot 5H_2O$ purged with N_2 was slowly added to the rest of the reagents, and this step took approximately 30 min. The color of the solution was dark purple at this stage. The round bottom flask was then placed in an oil bath at 150 ℃ and refluxed for 90 minutes. After 90 min, the solution was allowed to cool to room temperature, centrifuged several times at 3000 rpm for 5 minutes and then washed in water and ethanol to remove DMSO and any unreacted species.

In the $BiVO_4$ synthetic procedure, $Bi(NO_3)_3 \cdot 5H_2O$ (0.5 mmol) and NH_4VO_3 (0.5 mmol) were dissolved in 5 mL of nitric acid and 5 mL of distilled water. The mixed solution (20 μL) was dropped twice onto the FTO surface with 1 cm × 1 cm area. After being dried, the film was calcined at 500 ℃ for 2 h with the ramping rate of 2 ℃/ min.

The $AgFeS_2/BiVO_4$ composites were prepared via dropping the $AgFeS_2$ suspension onto the $BiVO_4$ film. Firstly, 4 mg $AgFeS_2$ was added into 200 μL ethanol with constant stirring. After being stirred for 24 hrs, the $AgFeS_2$ suspension was dropped onto the $BiVO_4$ film. The amount of $AgFeS_2$ addition were 10, 20, 30, 40 and 50 μL, and the corresponding $AgFeS_2/BiVO_4$ samples were labeled as AB-10, AB-20, AB-30, AB-40 and AB-50, respectively. The $AgFeS_2$/FTO film was prepared by adding $AgFeS_2$ suspension onto FTO film until it was fully covered with $AgFeS_2$ sample.

Characterization of samples: The X-ray diffraction (XRD) patterns were measured by a Bruker D8 Advance X-ray diffractometer with Cu K radiation. The accelerating voltage and applied current were 40 kV and 40 mA, respectively. UV−vis diffuse reflectance spectra of samples were collected by an UV−vis−NIR spectrometer (UV-2600, Shimadzu co., Japan) with $BaSO_4$ as the background and in the range 200−800 nm. The general morphologies and element mapping of the products were examined by field emission scanning electron microscopy (FESEM) on a Sigma Zeiss 150 (Cal Zeiss Co., Germany) instrument operated at 5 kV. The photoelectrochemical data was collected by a CHI-660E electrochemical workstation (Chenhua Instruments, Co., Shanghai). The photoelectrochemical experiment was carried out in a conventional three-electrode system with a quartz cell. A platinum wire and an Ag/AgCl electrode were used as the counter and reference electrodes, respectively. The electrolyte was 0.1 M Na_2SO_4 solution.

Photoelectrochemical Measurement: The photoelectrochemical characterization was performed with the CHI-660E electrochemical workstation under illumination by a 300 W Xe lamp (CEL-S500, Beijing Jin Yuan science and Technology Co., China) equipped with the AM 1.5G filter (light intensity: 100 mW/cm^2). The incident-photon-to-current-conversion efficiency (IPCE) was measured by interposing a monochromator (7ISW15, Beijing 7-Star Optical Instruments Co., China) between the xenon lamp and the photoelectrochemical cell. The monochromatic light was filtered by filter plates for different wavelengths with a

bandwidth of 10 nm, and the monochromatic light power density was measured by a UV-vis irradiatometer (CEL-NP2000, Beijing Jin Yuan science and Technology Co., China) with an accuracy of 1 $\mu W/cm^2$.

Supporting Information

Supporting Information is available from the Wiley Online Library or from the author.

Acknowledgement

The authors gratefully acknowledge financial support from National Nature Science Foundation of China (No. 21507011), an Eastern Scholar Program (SSH1829002 to L.Z.) and the Thousand Young Talents Program to L. Z. This work is part of the research program of the Foundation for Fundamental Research on Matter (FOM), which is part of the Netherlands Organization for Scientific Research (NWO). The authors acknowledge financial support from the European Research Council under the European Union's Seventh Framework Programme (FP/2007-2013)/ERC Grant Agreement no. 337328, "NanoEnabledPV".

Received: ((will be filled in by the editorial staff))
Revised: ((will be filled in by the editorial staff))
Published online: ((will be filled in by the editorial staff))

[1] A. Fujishima, K. Honda, *Nature* **1972**, *238*, 37-38.
[2] L. Zhang, D. Bahnemann, *ChemSusChem* **2013**, *6*, 283-290.
[3] L. Zhang, C. Baumanis, L. Robben, T. Kandiel, D. Bahnemann, *Small* **2011**, *7*, 2714-2720.
[4] X. Zheng, D. Li, X. Li, L. Yu, P. Wang, X. Zhang, J. Fang, Y. Shao, Y. Zheng, *Phys. Chem. Chem. Phys.* **2014**, *16*, 15299-15306.
[5] X. Ba, L.-L. Yan, S. Huang, J. Yu, X.-J. Xia, Y. Yu, *J. Phys. Chem. C* **2014**, *118*, 24467-24478.
[6] Y. Park, K. J. McDonald, K. S. Choi, *Chem. Soc. Rev.* **2013**, *42*, 2321-2337.
[7] A. Kudo, K. Ueda, H. Kato, I. Mikami, *Catal. Lett.* **1998**, *53*, 229-230.
[8] A. Kudo, K. Omori, H. Kato, *J. Am. Chem. Soc.* **1999**, *121*, 11459-11467.
[9] F. F. Abdi, L. Han, A. H. Smets, M. Zeman, B. Dam, R. van de Krol, *Nat. Commun.* **2013**, *4*, 2195.
[10] H. Ye, J. Lee, J. S. Jang, A. J. Bard, *J. Phys. Chem. C* **2010**, *114*, 13322-13328.
[11] C. Li, P. Zhang, R. Lv, J. Lu, T. Wang, S. Wang, H. Wang, J. Gong, *Small* **2013**, *9*, 3951-3956.
[12] Y. Hu, D. Li, Y. Zheng, W. Chen, Y. He, Y. Shao, X. Fu, G. Xiao, *Appl. Catal. B-Environ.* **2011,** *104*, 30-36.
[13] L. Zhang, C. Y. Lin, V. K. Valev, E. Reisner, U. Steiner, J. J. Baumberg, *Small* **2014**, *10*, 3970-3978.

[14] L. Zhang, E. Reisner, J. J. Baumberg, *Energy Environ.Sci.* **2014**, *7*, 1402.
[15] W. Luo, Z. Yang, Z. Li, J. Zhang, J. Liu, Z. Zhao, Z. Wang, S. Yan, T. Yu, Z. Zou, *Energy Environ.Sci.* **2011**, *4*, 4046.
[16] K. J. McDonald, K.-S. Choi, *Energy Environ.Sci.* **2012**, *5*, 8553.
[17] Y. Liang, T. Tsubota, L. P. A. Mooij, R. van de Krol, *J. Phys. Chem. C* **2011**, *115*, 17594-17598.
[18] W. J. Jo, J. W. Jang, K. J. Kong, H. J. Kang, J. Y. Kim, H. Jun, K. P. Parmar, J. S. Lee, *Angew. Chem. Int. Ed*. **2012**, *51*, 3147-3151.
[19] K. P. S. Parmar, H. J. Kang, A. Bist, P. Dua, J. S. Jang, J. S. Lee, *ChemSusChem* **2012**, *5*, 1926-1934.
[20] D. K. Zhong, S. Choi, D. R. Gamelin, *J. Am. Chem. Soc*. **2011**, *133*, 18370-18377.
[21] S. K. Pilli, T. G. Deutsch, T. E. Furtak, J. A. Turner, L. D. Brown, A. M. Herring, *Phys. Chem. Chem. Phys.* **2012**, 14, 7032-7039.
[22] S. Kohtani, J. Hiro, N. Yamamoto, A. Kudo, K. Tokumura, R. Nakagaki, *Catal. Commun.* **2005**, *6*, 185-189.
[23] H.-q. Jiang, H. Endo, H. Natori, M. Nagai, K. Kobayashi, *Mater. Res. Bull.* **2009**, *44*, 700-706.
[24] L. Yu, R. S. Kokenyesi, D. A. Keszler, A. Zunger, *Adv.Energy Mater.* **2013**, *3*, 43-48.
[25] B. Sciacca, A. O. Yalcin, E. C. Garnett, *J Am Chem Soc*, **2015**, *137*, 4340-4343.
[26] S. K. Han, C. Gu, M. Gong, Z. M. Wang, S. H. Yu, *Small*, **2013**, *9*, 3765-3769.
[27] M. Zhou, J. Bao, Y. Xu, J. Zhang, J. Xie, M. Guan, C. Wang, L. Wen, Y. Lei, Y. Xie, *ACS nano*, **2014**, *8*, 7088-7098.
[28] M. A. Butler, *J. Appl.Phys.* **1977**, *48*, 1914-1920.
[29] Y. Park, K. J. McDonald, K. S. Choi, *Chem.Soc. Rev.* **2013**, 42, 2321-2337.
[30] C. Martinez Suarez, S. Hernández, N. Russo, *Appl. Catal. A-Gene.* **2015**, *504*, 158-170.
[31] J. Wang, P. Wang, Y. Cao, J. Chen, W. Li, Y. Shao, Y. Zheng, D. Li, *Appl. Catal. B-Environ.* **2013**, *136-137*, 94-102.
[32] A. Hagfeldt, H. Lindström, S. Södergren, S.-E. Lindquist, *J. Electroanal. Chem.* **1995**, *381*, 39-46.
[33] N. J. Bell, Y. H. Ng, A. Du, H. Coster, S. C. Smith, R. Amal, *J. Phys. Chem. C* **2011**, *115*, 6004-6009.
[34] X. Yang, A. Wolcott, G. Wang, A. Sobo, R. C. Fitzmorris, F. Qian, J. Z. Zhang, Y. Li, *Nano lett.* **2009**, *9*, 2331-2336.
[35] A. Murphy, P. Barnes, L. Randeniya, I. Plumb, I. Grey, M. Horne, J. Glasscock, *Int. J. Hydrogen Energ.* **2006**, *31*, 1999-2017.
[36] Y. Xu, M. A. A. Schoonen, *Am. Mineral.* **2000**, *85*, 543-556.
[37] M. Long, W. Cai, J. Cai, B. Zhou, X. Chai, Y. Wu, *J. Phys. Chem. B* **2006**, *110*, 20211-20216.
[38] M. A. Butler, *J. Electrochem. Soc.* **1978**, *125*, 228.
[39] D. Hidalgo, S. Bocchini, M. Fontana, G. Saracco, S. Hernandez, *RSC Adv.*, **2015**, *5*, 49429-49438.
[40] P. Akhter, M. Hussain, G. Saracco, N. Russo, *Fuel*, **2015**, *149*, 55–65.
[41] J. R. Harbour, J. Tromp, M. L. Hair, *Can. J. Chem.*, **1985**, *63*, 204–208.
[42] B. Jenny, P. Pichat, *Langmuir*, **1991**, *7*, 947–954.
[43] I. Ilisz, K. F¨ oglein, A. Dombi, *J. Mol. Catal. A: Chem.*, 1998, *135*, 55–61.
[44] A. Lamberti, A. Sacco, D. Hidalgo, S. Bianco, D. Manfredi, M. Quaglio, E. Tresso, C. F. Pirri, *Acta Phys. Pol., A*, **2013**, *123*, 376.
[45] S. Hern´ andez, V. Cauda, A. Chiodoni, S. Dallorto, A. Sacco, D. Hidalgo, E. Celasco, C. F. Pirri, *ACS Appl. Mater. Interfaces*, **2014**, *6*, 12153–12167.

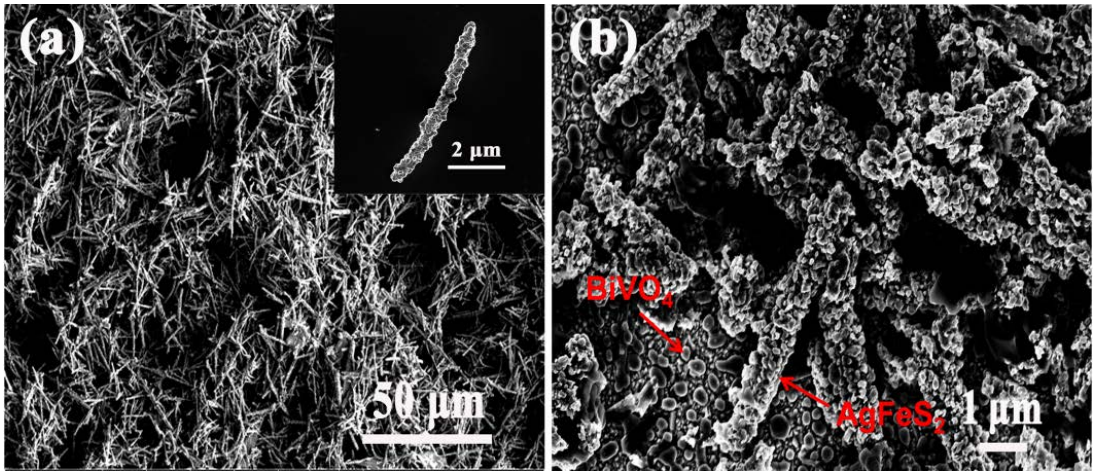

Figure 1. SEM images of $AgFeS_2$ nanowires (a) and AB-40 composite (b).

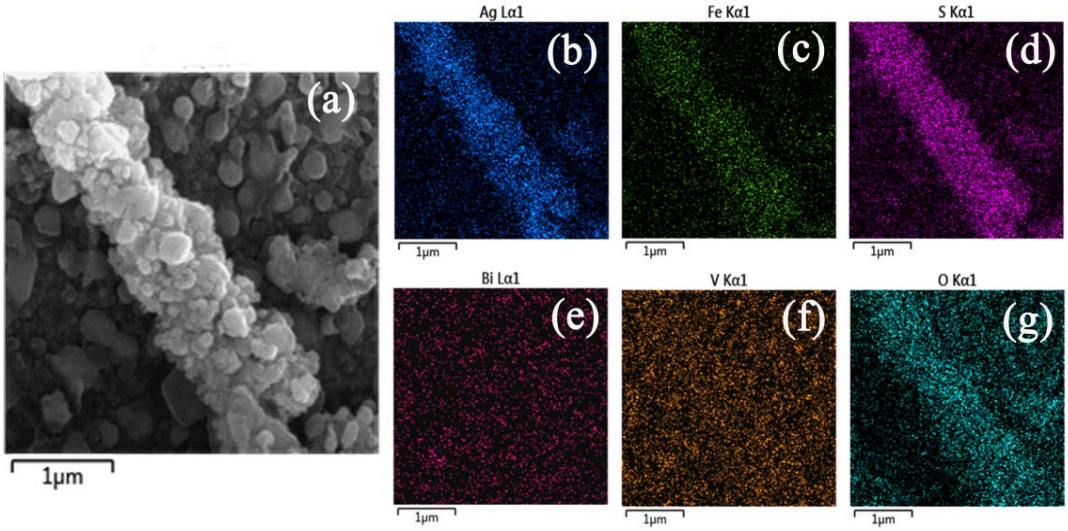

Figure 2. SEM image and EDX characterizations of AB-40 sample: (a) High-magnification SEM image; (b−g) Element mapping of Ag, Fe, S, Bi, V and O, respectively.

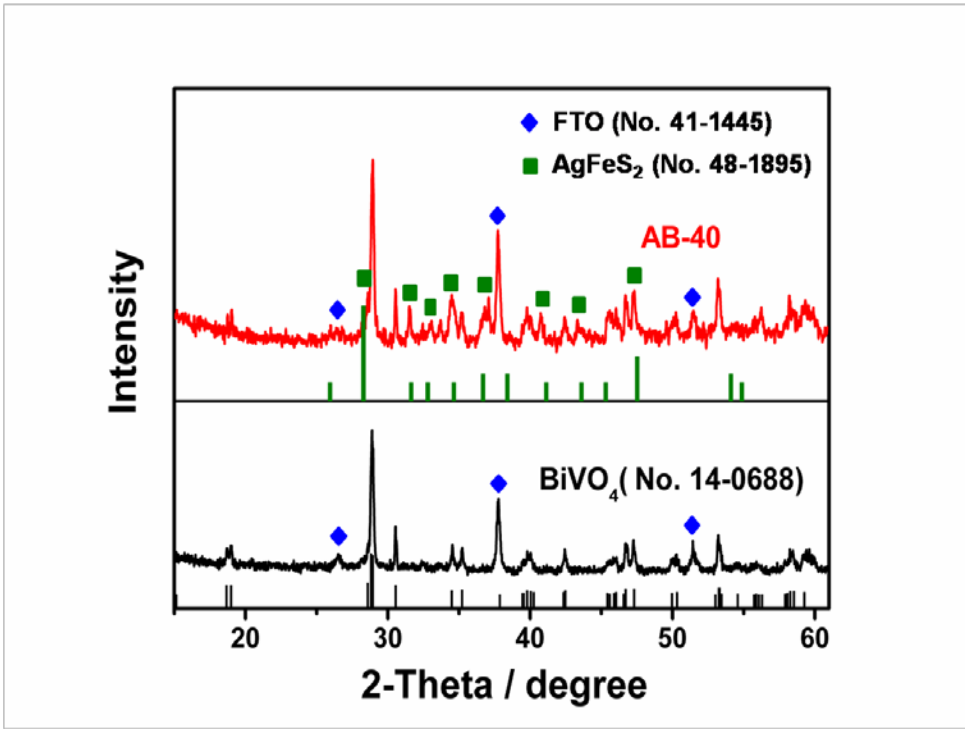

Figure 3. XRD patterns of $BiVO_4$ and AB-40.

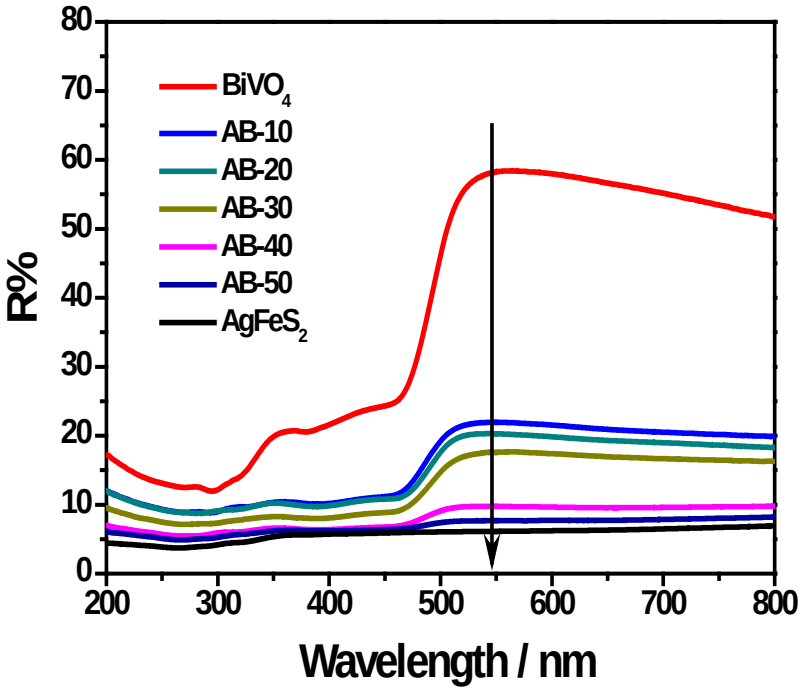

Figure 4. UV−vis diffuse reflectance spectra of $AgFeS_2$, $BiVO_4$ and $AgFeS_2/BiVO_4$ composites with different $AgFeS_2$ contents.

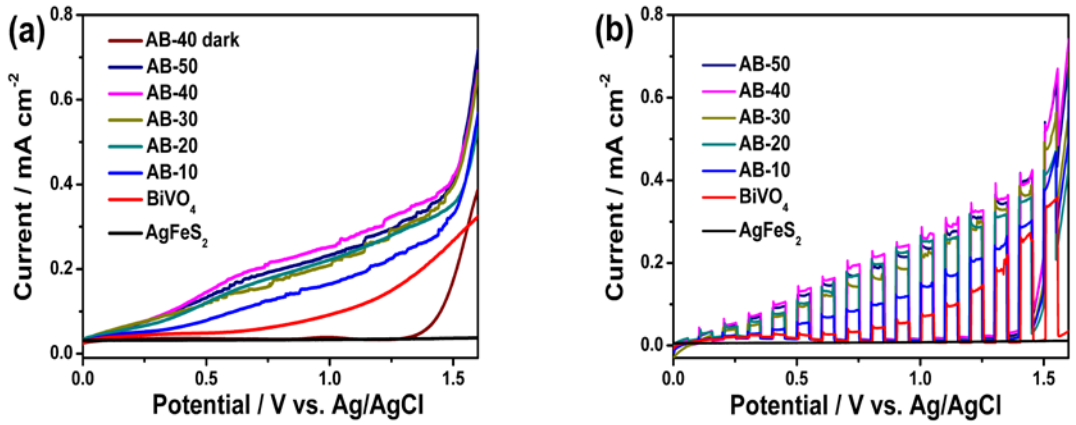

Figure 5. Photocurrent generation versus bias potential (vs. Ag/AgCl) obtained from $AgFeS_2$, $BiVO_4$ and $AgFeS_2/BiVO_4$ composites without being chopped (a) and chopped (b) in 0.1 M Na_2SO_4 under AM 1.5 G illuminations (100 mW/cm^2).

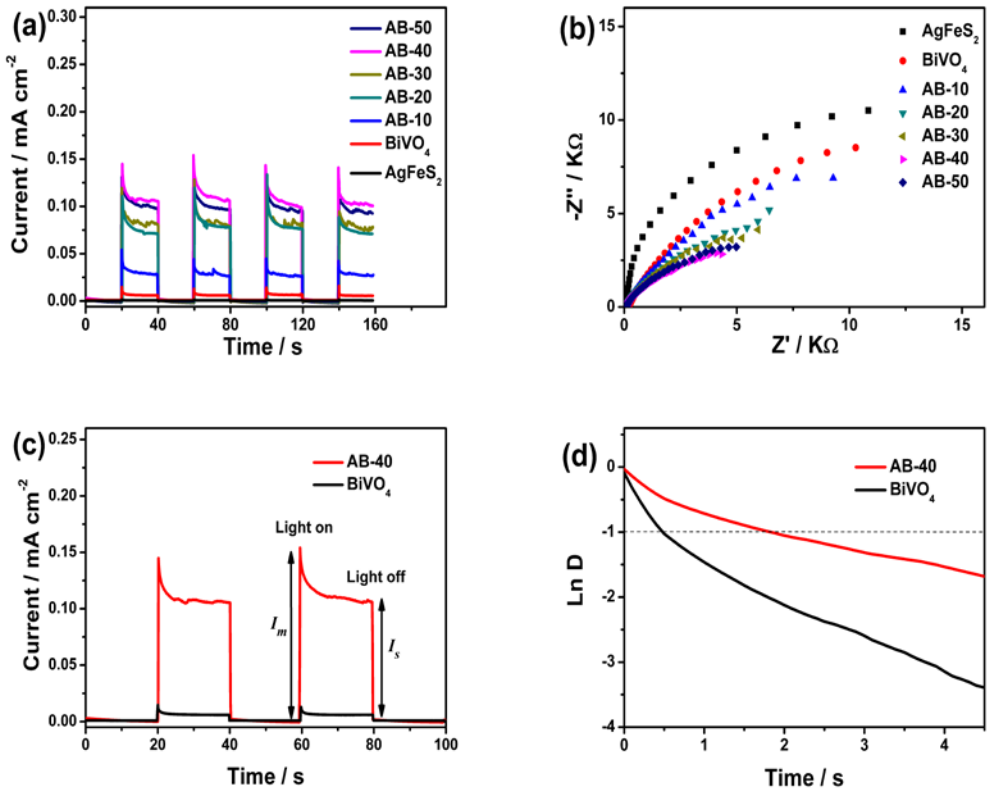

Figure 6. (a) Photocurrent spectra and (b) EIS Nynquist plots of $AgFeS_2$, $BiVO_4$ and $AgFeS_2/BiVO_4$ with an applied bias potential of 0.6 V vs. Ag/AgCl under AM 1.5 G illuminations (100 mW/cm^2). (c) Transient photocurrent decay and (d) Transient decay times of $BiVO_4$ film and AB-40 electrodes (see text for definition of parameter D).

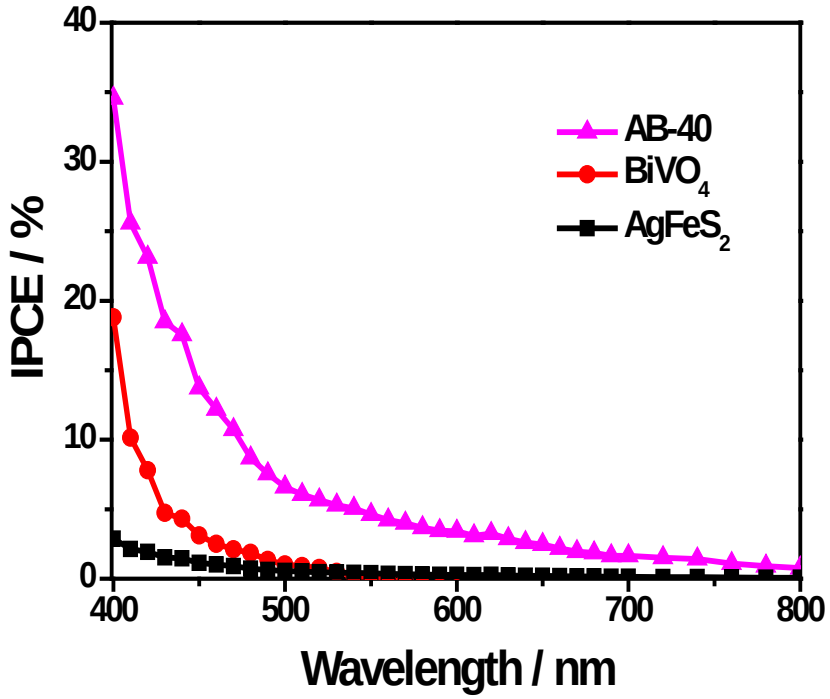

Figure 7. Measured IPCE spectra of $AgFeS_2$, $BiVO_4$ and AB-40 in the region of 400 to 800 nm at a potential of +0.6 V under AM 1.5 G illuminations (100 mW/cm^2), respectively.

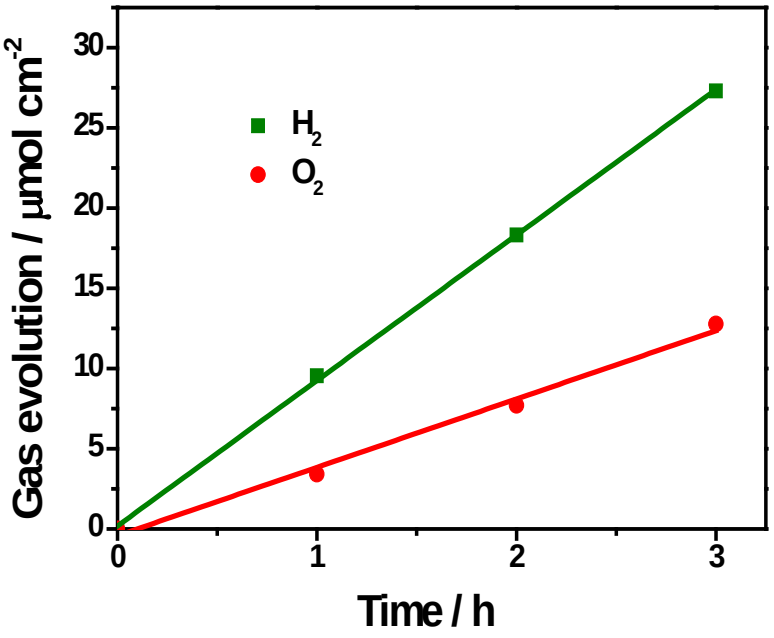

Figure 8. Gas evolution of the AB-40 photoanode at an applied potential of 1.6 V (vs Ag/AgCl) under AM 1.5 G illuminations (100 mW/cm^2).

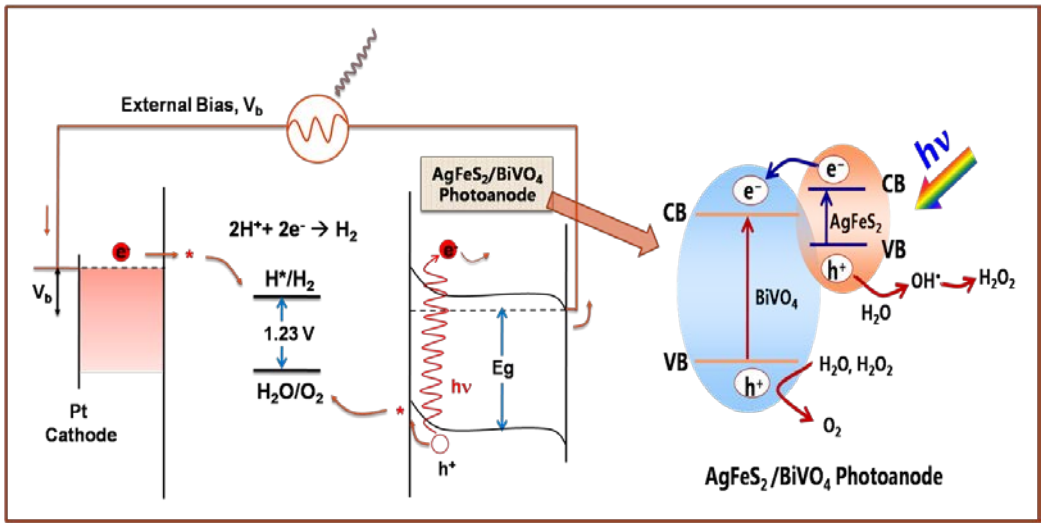

Figure 9. Mechanism of UV-Vis light absorption and charges transfer in $AgFeS_2/BiVO_4$ composite films for the photoelectrochemical water splitting reaction.

Table 1. Absolute electronegativity, energy band gap, calculated conduction band and valance band edge versus normal hydrogen electrode (NHE) at the point of zero charge for $AgFeS_2$ and $BiVO_4$ semiconductors.

Semiconductor	Absolute electronegativity (χ) (eV)	Calculated conduction band edge (eV)	Calculated valance band edge (eV)	Energy band gap E_g (eV)
$AgFeS_2$	5.14	0.04	0.92	0.88
$BiVO_4$	6.04	0.38	2.70	2.32

A novel ternary sensitizer $AgFeS_2$ is used to optimized $BiVO_4$ for photoelectrochemical water splitting to enhance the solar-to-hydrogen conversion efficiency. $AgFeS_2$ /$BiVO_4$ composite electrode is found to be promising for solar water splitting, which possesses extended light absorption spectrum and improved charge separation and collection efficiency.

ternary sensitizer, extended light absorption, PEC, composite, solar-to-hydrogen

X. Zheng[a], B. Sciacca[b], E. C. Garnett[b]*, L. Zhang[a]*

$AgFeS_2$ Modified $BiVO_4$ Photoanode for Photoelectrochemical Water Splitting

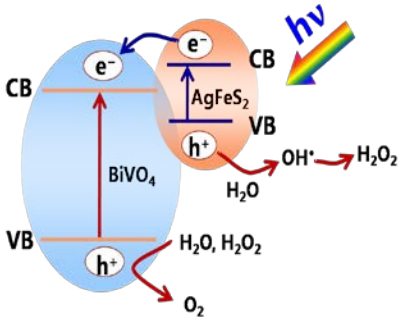

CHEMPLUSCHEM

Supporting Information

$AgFeS_2$-Nanowire-Modified $BiVO_4$ Photoanodes for Photoelectrochemical Water Splitting

Xiuzhen Zheng,[a] Beniamino Sciacca,[b] Erik C. Garnett,*[b] and Liwu Zhang*[a]

cplu_201600095_sm_miscellaneous_information.pdf

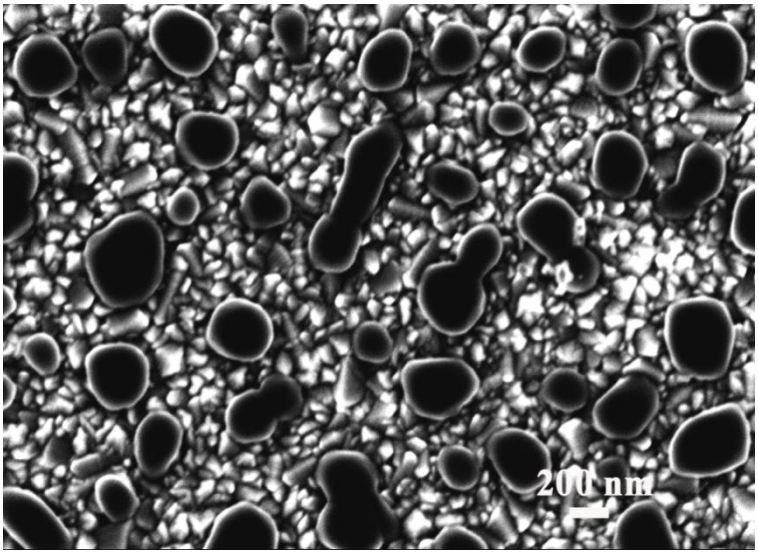

Figure S1. SEM images of $BiVO_4$.

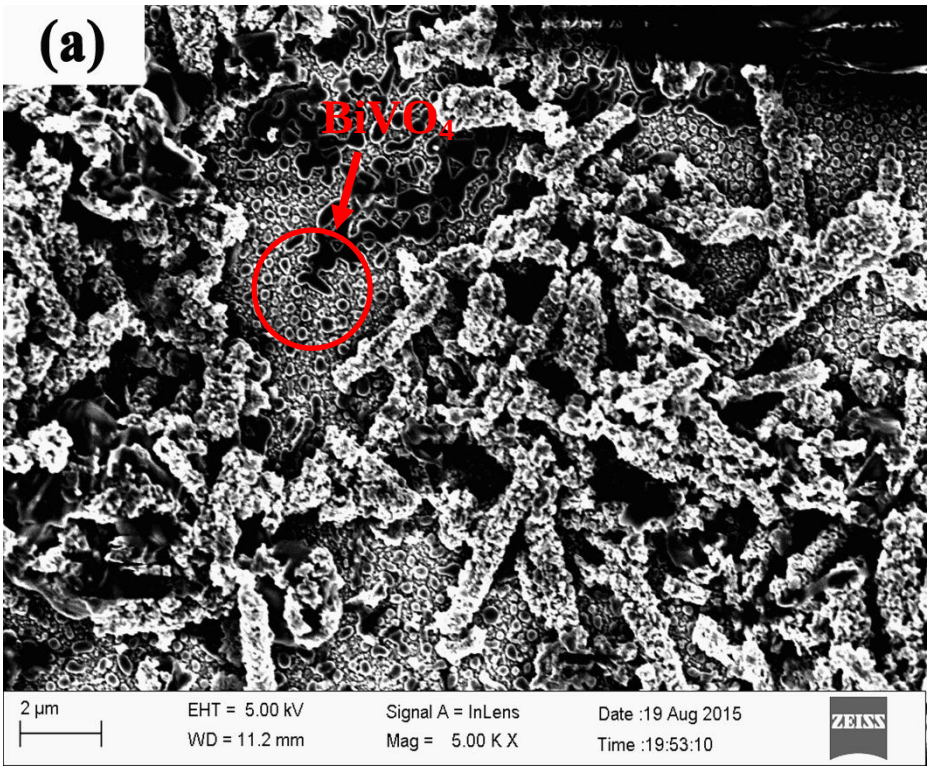

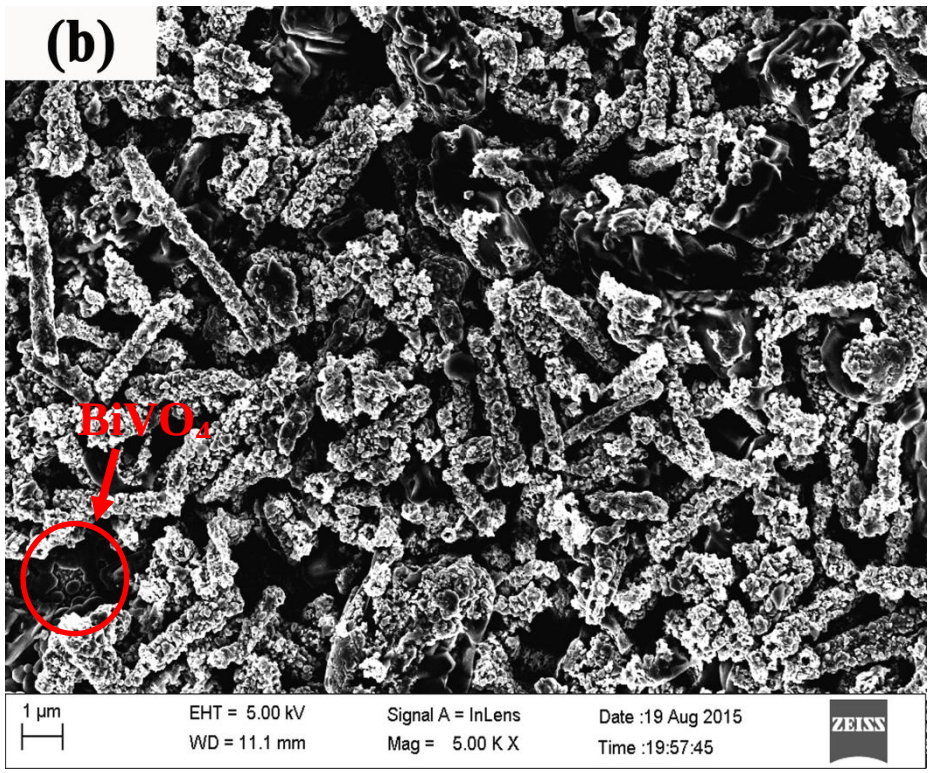

Figure S2. SEM images of AB-40.

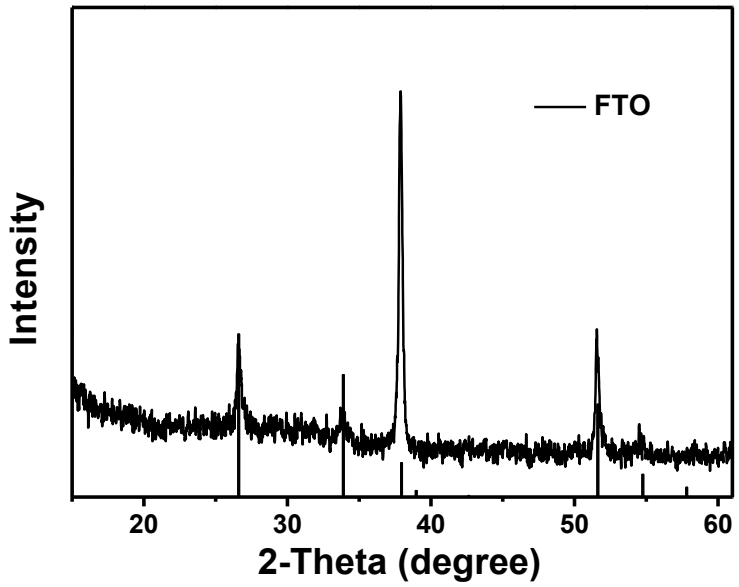

Figure S3. XRD pattern of FTO (JCPDS No. 41-1445).

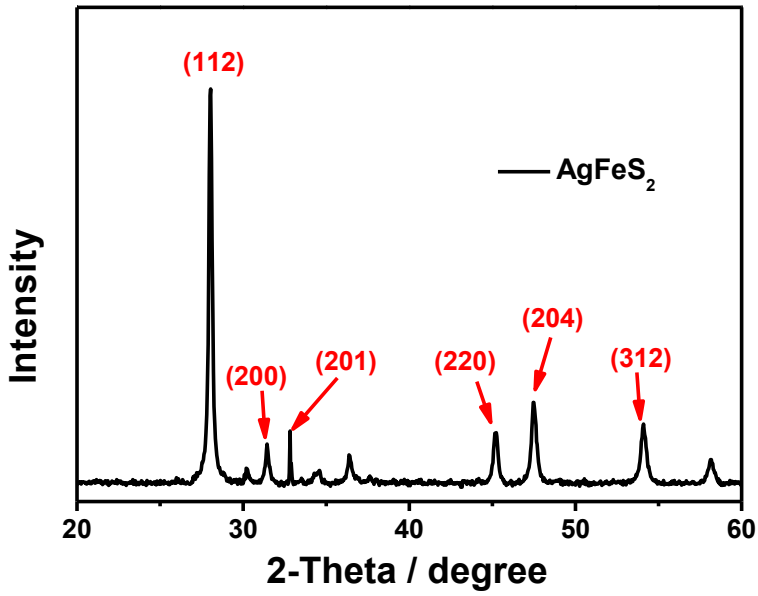

Figure S4. XRD pattern of $AgFeS_2$ (JCPDS No. 48-1895).

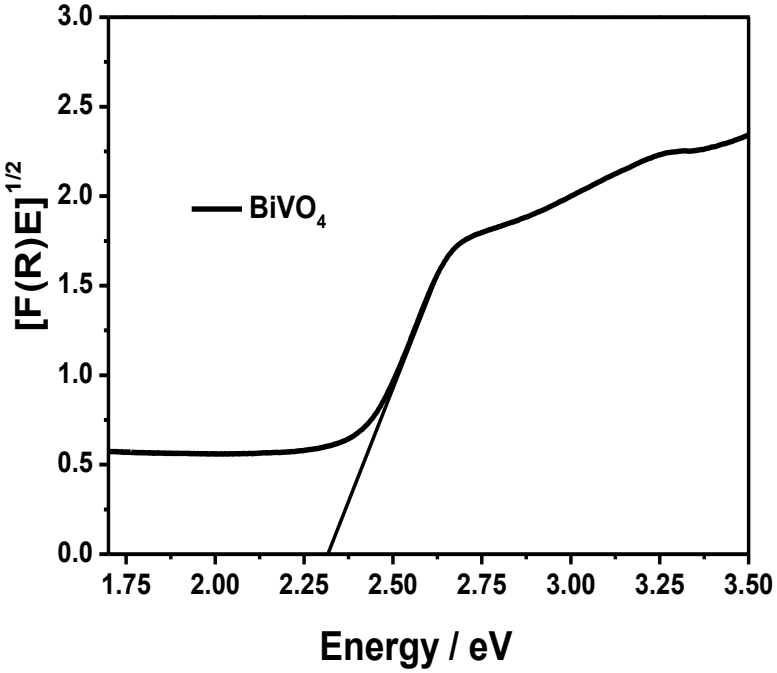

Figure S5. Optical band gap energy (E_g) of $BiVO_4$.

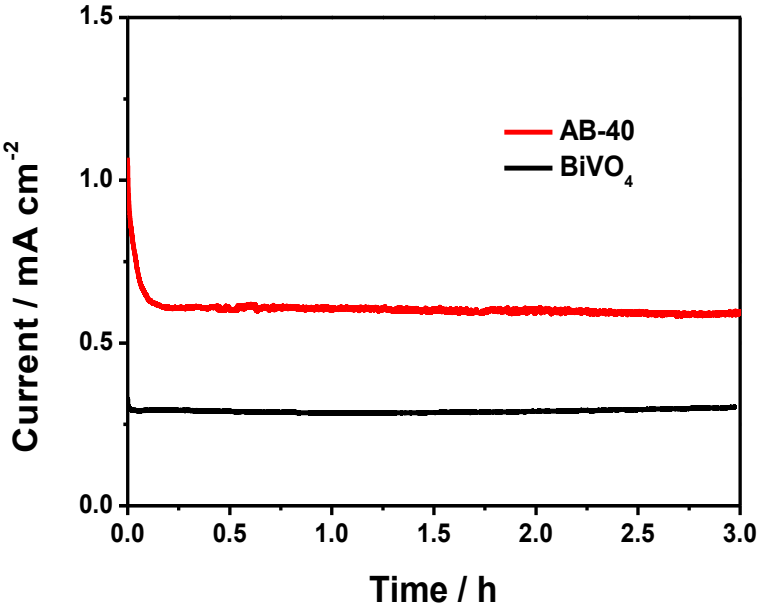

Figure S6. Current density vs time for AB-40 electrode at an applied potential of 1.6 V (vs Ag/AgCl) under AM 1.5 G illuminations (100 mW/cm^2).

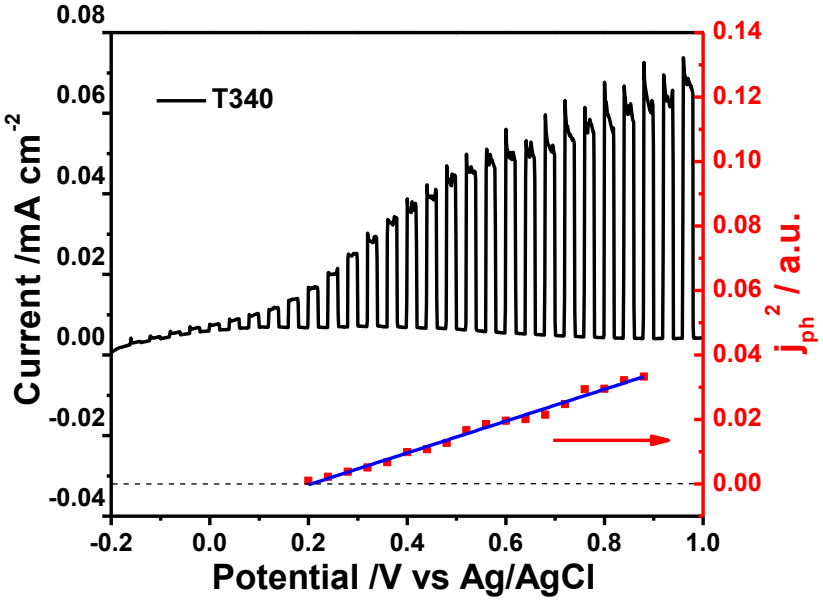

Figure S7. E_{FB} measurements of $BiVO_4$ by the photocurrent (j_{ph}) onset method using the fit to Buttler theory for j_{ph}^2 in the mixture of the electrolyte of 1 mol/L Na_2SO_4 and 1 mol/L AcOK under simulated solar light illumination (a scan rate of 1 mV/s, scanned from positive side, and a light intensity of 100 mW/cm^2).

The position of the semiconductor band is an important physical property of the semiconductor. Herein, the flat band potential (E_{FB}) is measured using the photocurrent onset potential for $BiVO_4$ film.[S1] Typically, when the surface of the semiconductor electrode and the solution interface are contacted, the surface band bends to form a built-in electric field. According to the mechanism of photocurrent, photo-generated electrons migrate to form the photocurrent in the effect of built-in electric field. When a reverse bias is applied, it can offset the part of the built-in electric field. As the built-in voltage approaches zero, the current is zero, and the external voltage at this time is equal to the flat band. Therefore, ignoring the deviation of the flat band and the conduction band potential, it can be considered that the position of the conduction band is approximated by the position of the flat band potential.

E_{FB} is measured using the photocurrent onset potential for $BiVO_4$ film in aqueous solution. Figure 10 shows the photocurrent of $BiVO_4$ film in a mixture of the electrolyte of 1 mol/L

Na_2SO_4 and 1 mol/L AcOK with simulated solar light (100 mW/cm^2). By alternating light and dark measures of linear sweep photovoltammetry, a step change could be measured by photocurrent density (j_{ph}) with the scan. From the onset of j_{ph}, the Buttler method is used to calculate E_{FB} using equation ($j_{ph}^2 \sim (E - E_{FB})$), where j_{ph}^2 is proportional to potential E.[S1, S2] The square of the j_{ph} vs. E would have an x intercept of E_{FB}. As shown in Figure S7, E_{FB} of $BiVO_4$ is 0.20 eV vs. Ag/AgCl. To further calculate, it is 0.40 eV vs. NHE. Thereby, E_{CB} of $BiVO_4$ is about 0.40 eV. As the band gap for $BiVO_4$ is evaluated as 2.32 eV from the UV-vis spectrum, according to the formula $E_g = E_{VB} - E_{CB}$, the corresponding valence band potentials for $BiVO_4$ film is about 2.7 eV. Therefore, the value of E_{CB} measured by photocurrent onset potential is accorded with the calculated result.

Reference:

[S1] M. A. Alpuche-Aviles; Wu Y., *J Am Chem Soc* **2009,** *131*, 3216-24.

[S2] M. A. Butler, *J.Appl.Phys.* **1977**, *48*, 1914-1920.